Topics in Catalysis Vol. 35, Nos. 1–2, June 2005 (© 2005)
DOI: 10.1007/s11244-005-3809-1

Ordered mesoporous materials with improved stability and catalytic activity

Feng-Shou Xiao

Department of Chemistry and State Key Laboratory for Inorganic Synthesis and Preparative Chemistry, Jilin University, Changchun 130023, P.R. China

Microporous crystals of zeolites such as Y, Beta, and ZSM-5 are widely used commercial catalysts, but their applications are strongly limited by their small pore sizes. Recent progress in solving this is used to ordered mesoporous materials such as MCM-41, HMS, and SBA-15. These mesoporous materials have pore diameters of 2.0–30 nm and exhibit good catalytic properties for the catalytic conversion of bulky reactants. However, when compared with microporous crystals of zeolites, the catalytic activity and hydrothermal stability are relatively low, which severely hinders their practical applications in industrial catalytic reactions such as petroleum cracking. The relatively low catalytic activity and hydrothermal stability can be attributed to the amorphous nature of the mesoporous walls. In this account, we systemically review the routes for improving catalytic activity and hydrothermal stability of mesoporous materials, which include (1) acidic sulfated zirconia supported in mesoporous materials; (2) strongly acidic and thermally stable mesostructured sulfated zirconia with tetragonal crystalline phase; (3) strongly acidic and hydrothermally stable mesoporous aluminosilicates synthesized in alkaline media; (4) strongly acidic and hydrothermally stable mesoporous aluminosilicates synthesized in strongly acidic media; (5) hydrothermally stable mesoporous titanosilicates with catalytically active titanium species in oxidations; (6) high-temperature generalized synthesis of ultrastable ordered mesoporous silica-based materials by using fluorocarbonhydrocarbon surfactant mixtures.

KEY WORDS: hydrotherma1 stability; ordered mesoporous materials; acidity; oxidation; high-temperature hydrothermal synthesis; preformed nanosized zeolite precusors; aluminosilicate; titanosilicate.

1. Introduction

Since the first discovery of ordered mesoporous materials by Mobil scientists [l], a series of novel ordered mesoporous materials have been successfully synthesized [2–16]. These mesoporous materials exhibit much higher surface area (600–1300 m^2/g), and larger pore size (2–30 nm), exhibiting widely potential applications in industrial catalytic reactions, compared with microporous crystals of zeolites [2]. But unfortunately, these mesoporous materials have relatively low catalytic activity and hydrothermal stability, which severely hinders their practical applications in catalysis [2]. The relatively low catalytical activities of mesoporous materials such as MCM-41, as compared to microporous crystals of zeolites, can be typically attributed to the low acidity or low oxidation ability of catalytically active species, which is strongly related to the amorphous nature of the pore walls [1,2]. Therefore, increasing acidity, oxidation ability, and hydrothermal stability are great tasks for rational syntheses of ordered mesoporous materials.

In this account, we have reviewed our recent development for rational syntheses of mesoporous materials with improved catalytic activity and hydrothermal stability, which include (1) acidic sulfated zirconia supported in mesoporous materials; (2) strongly acidic and thermally stable mesporous sulfated zirconia with tetragonal crystalline phase; (3) strongly acidic and hydrothermally stable mesoporous aluminosilicates synthesized in alkaline media; (4) strongly acidic and hydrothermally stable mesoporous aluminosilicates synthesized in strongly acidic media; (5) hydrothermally stable mesoporous titanosilicates with catalytically active titanium species in oxidations; (6) high-temperature generalized synthesis of stable ordered mesoporous silica-based materials by using fluorocarbon–hydrocarbon surfactant mixtures.

To whom correspondence should be addressed.
Email: fsxiao@mail.jlu.edu.cn

2. Sulfated zirconia supported into mesoporous materials

It is well known that sulfated zirconia is a superacid catalyst characterized by Hammett indicators [17,18], which is suitable for catalyzing reactions such as hydrocarbon isomerization and etherification [19–21]. Supporting sulfated zirconia in the mesopores is one of the good ways for increasing acidity of mesoporous materials, and recently these works have been investigated extensively [22–26].

Matsuhashi *et al.* [22] reported that a mesoporous solid acid with ordered mesopores was prepared by modification of FMS-16 with sulfated zirconia ($[SO_4^{2-}]/ZrO_2$/FMS-16). FMS-16 precalcined at 850 °C was soaked with an ethanol solution of zirconyl chloride, followed by exposure of H_2SO_4 and calcination at 650 °C in air. X-ray diffraction measurement shows that $[SO_4^{2-}]/ZrO_2$/FMS-16 basically retains its ordered mesostructure. Nitrogen isotherms of the samples show that the surface area and pore volume of $[SO_4^{2-}]/ZrO_2$/FMS-16 reduce significantly as compared with those of unmodified FMS-16, indicating that some pores are blocked by $[SO_4^{2-}]/ZrO_2$ species.

Kawi *et al.* [23] reported the preparation of superacid catalyst $[SO_4^{2-}]/ZrO_2$/MCM-41. In this case, pre-dried silica MCM-41 was dispersed into a mixed solution of $Zr(OPr^n)_4$ and *n* -hexane under vigorous stirring, followed by removal of organic solvent, hydrolysis by water at room temperature, immersion by H_2SO_4 , and calcination at 600 °C. Catalytic tests show that $[SO_4^{2-}]/ZrO_2$ /MCM-41 is ca. 2.5–3 times more active than the conventional $[SO_4^{2-}]/ZrO_2$ superacid catalyst for MTBE and *n* -pentane isomerization.

Mou *et al.* [24] also reported the synthesis of superacid of $[SO_4^{2-}]/ZrO_2$ supported on MCM-41 by using a one-step incipient wetness impregnation method with zirconium sulfate as the precursor in methanol solution, followed by thermal decompositon of the precursor in air.

Notably, the preparation of $[SO_4^{2-}]/ZrO_2$ supported on mesoporous materials is generally carried out in organic solution such as methanol and hexane because the impregnation of zirconium salts with mesoporous materials of MCM-41 and subsequent treatments usually take more than several hours at relative high temperature (100 °C), which may result in the destruction of mesostructures [22–24].

Recently, Xiao *et al.* [26] have prepared $[SO_4^{2-}]/ ZrO_2$ /MCM-41 by monolayer dispersion of $ZrOCl_2{\cdot}8H_2O$ into the mesopores, followed by the hydrolysis and sulfation. The results show that $ZrO_2/[SO_4^{2-}]$ was successfully loaded into the inner pores of MCM-41 and the as-synthesized catalyst showed favorable catalytic properties. In this case, $[SO_4^{2-}]/ZrO_2$/MCM-41 retained well-ordered mesoporous structures due to the

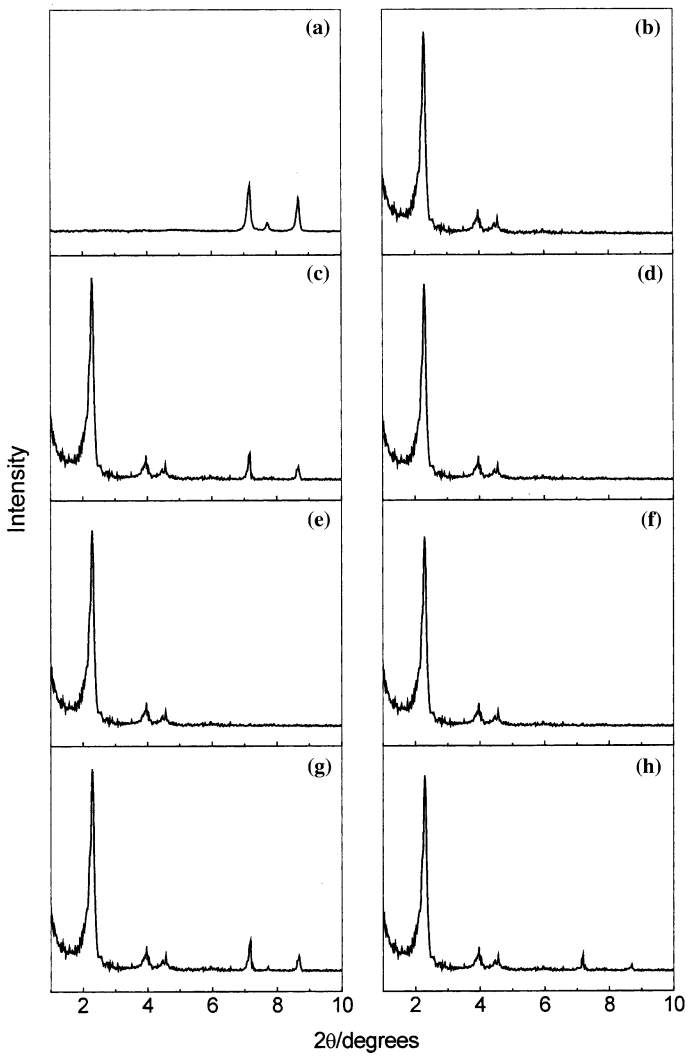

Figure 1. XRD patterns of (A) $ZrOCl_2{\cdot}8H_2O$ (B) MCM-41 (C) mechanical mixture of $ZrOCl_2{\cdot}8H_2O$ and MCM-41 ($ZrOCl_2{\cdot}8H_2O$/MCM-41 = 0.16 g/g Zr/Si = 0.063), (D) after C, the mixture was heated at 80 °C for 24 h, (E) after D, the sample was hydrolyzed in 0.5 M of $NH_3{\cdot}H_2O$ at room temperature, activated at 140 °C for 5 h, and sulfated in 0.5 M of H_2SO_4 at room temperature for 10 min, (F) mechanical mixture of $ZrOCl_2{\cdot}8H_2O$ and MCM-41 ($ZrOCl_2{\cdot}8H_2O$/MCM-41 = 0.23 g/g and Zr/Si = 0.084), followed by heating at 80 °C for 24 h, (G) mechanical mixture of $ZrOCl_2{\cdot}8H_2O$ and MCM-41 ($ZrOCl_2{\cdot}8H_2O$/MCM-41 = 0.34 g/g and Zr/Si = 0.126) for 20 min, (H) after G, the mixture was heated at 80 °C for 24 h. Reprinted with permission fron Ref [43].

avoidance of impregnating the mesoporous materials with zironium salt in aqueous solution.

Figure 1 shows XRD patterns in the region of 1–10° for $ZrOCl_2{\cdot}8H_2O$, MCM-41, and a mixture of $ZrOCl_2{\cdot}8H_2O$ and MCM-4l ground for 20 min as well as heated at 80 °C for 12 h, respectively. $ZrOC1_2{\cdot}8H_2O$ (figure 1A) exhibits two peaks at 7.1° and. 8.6°. MCM-41 (figure 1B) exhibits four peaks at 2.2°, 3.8°,4.4°, and 5.8°. The mixture of $ZrOCl_2{\cdot}8H_2O$ and MCM-41 (figure 1C) ground for 20 min exhibits both the peaks assigned to $ZrOCl_2{\cdot}8H_2O$ and the peaks assigned to MCM-41. Notably, after heating the mixture of $ZrOCl_2{\cdot}8H_2O$ and MCM-41 (figure 1D) at 80 °C for 12 h, the peaks at 7.1° and 8.6° assigned to crystalline $ZrOCl_2{\cdot}8H_2O$ disappear, indicating that $ZrOCl_2{\cdot}8H_2O$ becomes highly dispersed in the mesopores of MCM-41, i.e. $ZrOCl_2{\cdot}8H_2O$ no longer exists in crystalline state, which is in good agreement with the results published in literature [27].

For the samples treated by hydrolysis at room temperature for 5 min after dispersion of $ZrOC1_2 \cdot 8$-H_2O into the pores of mesoporous materials, activation at 140 °C for 5 h , sulfation at room temperature for 10 min, and calcination at 600 °C for 3 h (figure 1E), the characteristic peaks assigned to the hexagonal mesoporous materials are almost unchanged, and no peaks in the region of 30–50° assigned to ZrO_2 crystals could be observed. These results suggest that the mesostructured materials are stable and no ZrO_2 crystals are formed after the treatments of dispersion, hydrolysis, activation, sulfation, and calcination. Interestingly, although MCM-41 is not stable in boiling water, it is stable under the above treatments, suggesting that the solid dispersion method is useful for preparation of sulfated zirconia in the mesopores of MCM-41.

When the amount of $ZrOCl_2{\cdot}8H_2O$/MCM-41 was increased to 0.23 g/g (molar ratio of Zr/Si at 0.084), we still did not observe the XRD peaks of crystalline $ZrOCl_2{\cdot}8H_2O$, as shown in figure 1F. Upon further increase of $ZrOC1_2{\cdot}8H_2O$ loading in MCM-41 sample to over 0.23 g/g, the characteristic peaks assigned to $ZrOC1_2{\cdot}8H_2O$ appeared again, indicating the presence of crystalline $ZrOCl_2{\cdot}8H_2O$ in the sample, as given in figure 1G and 1H. These results indicate that the maximum content of $ZrOC1_2{\cdot}8H_2O$ supported in MCM-41 is about 0.23 g/g.

Catalytic activities of various catalysts in cracking of cumene and 1,3,5-triisopropylbenzene are presented in table 1. In cumene cracking, MCM-41 is inactive (5.4%) because there is no acidic site in the MCM-41 sample. However, after supporting sulfated zirconia in the MCM-41 material (Zr/Si = 0.042), the sample activity ($[SO_4^{2-}]/ZrO_2$/MCM-41) increases significantly, giving a conversion of 69.3%, which is a little higher than that of HZSM-5 sample. In contrast, the same amount of sulfated zirconia mechanically mixed with MCM-41 (Zr/Si = 0.042) shows a very low conversion at 8.4%.

Table 1
Catalytic activities of various samples in cracking of cumene and 1,3,5-triiso1propylbenzene [26]

Sample	Si/Al	Cumene Conv. (%) at 250 °C	TIPB Conv. % at 250 °C
HMCM-41	∝	5.4	0.8
SZ + MCM-41 (mechanical mixture)	∝	8.4	16.8
SZ/MCM-41 (sulfated zirconia supported into mesopores)	∝	69.3	99.9
SZ (sulfated zirconia)		75.2	98.1
HZSM-5	60	68.4	2.7

TIPB: 1,3,5-triisopropylbenzene.

These results suggest the SZ/MCM-41 is much more active due to its larger surface area as compared with that of SZ.

In catalytic cracking of 1,3,5-triisopropylbenzene, MCM-41 is inactive; HZSM-5 has a very low conversion because of the small pore size of MFI zeolite. However, after supporting sulfated zirconia in MCM-41, the sample ($([SO_4^{2-}]/ZrO_2$/MCM-41) shows the highest catalytic activity (99.9%), which is much higher than that of the mechanical mixture of sulfated zirconia with MCM-41 (16.8%). These results suggest that SZ/MCM-41 is an excellent candidate for cracking catalyst of large molecules.

Notably, the amount of sulfated zirconia supported into mesoporous materials is limited because some pores are blocked by $([SO_4^{2-}]/ZrO_2$ an the surface areas of the materials is reduced significantly [26]. Moreover, the catalytic activity for *n*-butane isomerization (typical model reaction for superacid catalysts) over $([SO_4^{2-}]/ZrO_2$/MCM-41 reduces extensively [26] as compared with that over $([SO_4^{2-}]/ZrO_2$, which is reasonably assigned that the acidic strength of $([SO_4^{2-}]/ZrO_2$/MCM-41 is much lower than that of $([SO_4^{2-}]/ZrO_2$ due to the absence of tetragonal phase of crystalline ZrO_2 in the limited mesopores of MCM-41. Therefore, mesoporous sulfated zirconia with tetragonal crystalline phase is desirable.

3. Mesostructured sulfated zirconia with tetragonal crystalline phase

The mesostructured sulfated zirconia with tetragonal crystalline phase has been prepared from assembly of block copolymer surfactant (P123) with $ZrOCl_2 \cdot 8H_2O$, followed by crystallization of the sample in an autoclave, extraction of surfactant, immersion by $(NH_4)_2SO_4$ solution, and calcination [28].

The dependence of catalytic activity for *n*-butane isomerization on reaction time over conventional sulfated zirconia (SZ) and mesostructured sulfated zirconia (MSZ-5) show that MSZ-5 is much more active than SZ [28]. The acidic strength of MSZ-5 is measured

with Hammet indicator, giving the same H_0 value as that of SZ, which is much higher than that of $[SO_4^{2-}]/ZrO_2$/MCM-41 [28]. These results indicate that mesostructured sulfated zirconia (MSZ-5) with strongly acidic strength is successfully prepared.

XRD characterization shows that the as-synthesized MSZ-5 exhibits a broad peak at 1.01° in the small-angle region and a very broad peak at 25–35° in the wide-angle region. The peak at 1.01° is assigned to the mesostructure [1,2], and the very broad peak at 25–35° is assigned to the amorphous nature of zirconia. However, the as-calcined MSZ-5 shows both a peak at 0.89° in the small-angle region and obvious peaks at ca. 30°, 35°, 50° and 60° in the wide-angle region. The peaks in the wide-angle region are characteristic of the tetragonal phase of crystalline ZrO_2, suggesting that calcination of the as-synthesized mesostructured sulfated zirconia results in formation of crystalline ZrO_2 tetragonal phase, which is very important for the preparation of sulfated zirconia with strongly acidic sites [29].

Transmission electron on micrograph (TEM) of the as-calcined MSZ-5 is spotted with worm-like pore. Selected-area electron diffraction patterns recorded on the same sample confirm that the mesostructured walls are comprised of tetragonal phase, displaying characteristic diffuse electron diffraction rings.

N_2 isotherm of MSZ-5 shows a hysteresis loop at high relative pressure, which is related to the capillary condensation associated with mesopores. Correspondingly, BJH pore size distribution for MSZ-5 shows a mean value at 5.1 nm. Furthermore, a high BET surface area of 189 m^2/g is observed for MSZ-5, which is much larger than that for conventional SZ (80–100 m^2/g) [30].

Although the mesostructured sulfated zirconia with tetragonal crystalline phase (MSZ-5) is obtained, the thermal stability of its mesostructure and its anti-deactivation ability are still relatively poor, compared with the conventional sulfated zirconia [31].

To improve the lifetime of sulfated zirconia in catalysis, various promoters were introduced. At the beginning, the addition of small amounts of Fe and Mn [32,33], and Ni [34] is found to increase the activity in *n*-butane isomerization, but the catalysts still deactivate quickly. Recently, much attention has been paid on the sulfated zirconia promoted by A1 since it significantly enhances the catalytic activity and stability of sulfated zirconia [35,36].

We demonstrate here that the introduction of a little amount of A1 (3% mol. as Al_2O_3) into the walls of mesostructured sulfated zirconia (Al-MSZ-5) results in significant improvement of its mesostructural thermal stability. Sample characterization shows that the Al-promoted mesostructured sulfated zirconia exhibits higher catalytic activity and better anti-deactivation ability for *n*-butane isomerization than non-promoted mesostructured sulfated zirconia and conventional Al-promoted sulfated zirconia [37].

Figure 2 shows XRD patterns of MZS, MSZ-5, and Al-MSZ-5. The as-synthesized mesoporous zirconium sulfate (MZS) [36] shows three reflections (ca. 2.1°, 3.7° and 4.2°) in the small-angle region, but no reflections can be observed in wide angles (figure 2a). These results suggest that MZS is an ordered mesoporous material with amorphous walls. Nevertheless, after calcination at 550 °C for 3 h, the peaks in the small-angle region disappear completely, indicating that MZS has lost its mesostructure (figure 2b). This may be due to incomplete condensation of the walls in the synthesis of MZS [36]. In contrast, mesostructured sulfated zirconia (MSZ-5) [28] shows higher thermal stability, and it can

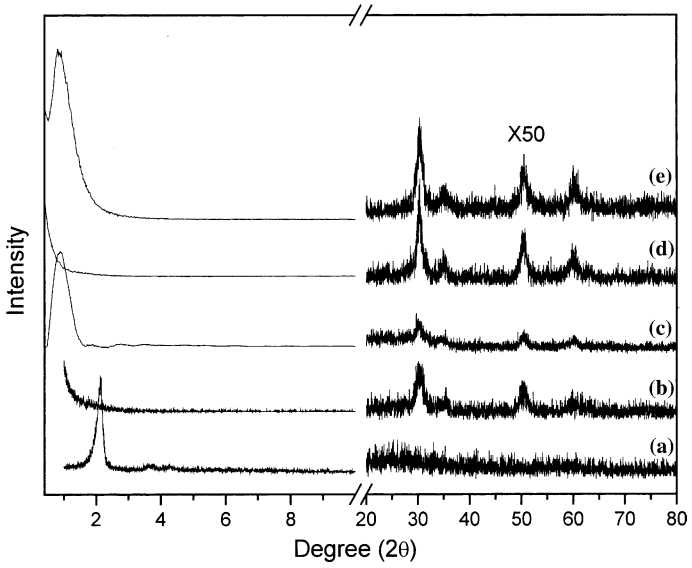

Figure 2. Small-angle and wide-angle XRD patterns of (a) as-synthesized MZS (b) MZS calcined at 550 °C for 3 h, (c) mesostructured sulfated zirconia (MSZ-5) (d) MSZ-5 calcined at 600 °C for 3 h, and (e) Al-MSZ-5 calcined at 650 °C for 3 h.

remain in its mesostructure after calcination at 550 °C (figure 2c). However, calcination at 600 °C leads to the loss of its mesostructure (figure 2d). Interestingly, after a little of Al is introduced into the mesostructured sulfated zirconia (Al-MSZ-5), its mesostructure is stable over 650 °C (figure 2e). Obviously, the presence of Al species can stabilize the mesostructure remarkably.

Catalytic activities for *n*-butane isomerization over MZS, MSZ-5, and Al-MSZ-5 are presented in table 2. Notably, mesoporous sulfated zirconia with amorphous walls (MSZ) [36] exhibits low catalytic activity (<1 mmol/g/h), although its surface area is relatively high (202 m^2/g). In contrast, conventional sulfated zirconia with tetragonal crystalline phase (SZ) gives high activity, reaching the values of 1.45–2.13 mmol/g/h after 5 min, even if the surface area is relatively low (84–112 m^2/g). Obviously, the presence of tetragonal crystalline phase in sulfated zirconia is one of the most important factors for high activity in *n* -butane isomerization.

Furthermore, we find that calcination temperature has a great effect on the activity of the catalyst for *n*-butane isomerization, and calcination at 650 °C is suitable for preparation of sulfated zirconia. For example, SZ calcined at 650 °C (2.13 mmol/g/h after 5 min) is more active than SZ calcined 55 °C (1.45 mmol/g/h after 5 min).

It is worthy to note that AI-SZ shows higher activity and stability than SZ, indicating that Al promoter plays a positive role in *n* -butane isomerization, in agreement with the results reported previously [35,36]. Most importantly, it is observed that Al-promoted mesostructured sulfated zirconia with tetragonal crystalline ZrO_2 (Al-MSZ-5) exhibits both the highest activity (4.29 mmol/g/h after 5 min) and the best anti-deactivation ability (3.26 mmol/g/h after 180 min) in all samples. This is reasonably assigned to the combination of advantages of large surface area, tetragonal crystalline, suitable calcination temperature, and positive effect of A1 promoter in mesostructured sulfated zirconia (Al-MSZ-5) [37].

4. Strongly acidic and hydrothermally stable mesoporous aluminosilicates synthesized in alkaline media

Notably, although mesoporous sulfated zirconia exhibits strongly acidic sites and high thermal stability, there are still many disadvantages for mesostructured sulfated zirconia including poor hydrothermal stability and relatively low surface area, compared with those of mesoporous aluminosilicates and microporous crystals of zeolites. Therefore, mesoporous aluminosilicates with strong acidity and uniform pore size as well as large surface area are still being sought.

Table 2
Catalytic activities in butane isomerization for 5 and 180 min on various samples

Samples	Calcination temp. (°C)	Activity (mmol/g/h)	
		5 min	180 min
SZ	550	1.45	1.05
SZ	650	2.13	1.43
MZS	540	< 1.0	< 1.0
MSZ-5	550	2.79	1.32
Al-SZ	650	3.79	2.71
Al-MSZ-5	650	4.29	3.26

It is well known that microporous crystals of zeolites are very stable, can be made to have high acidity and, hence, are widely used commercial catalysts, although their applications are intrinsically limited by their small channel diameters. Recently, there are several interesting reports on the synthesis of preformed zeolite nanoclusters with primary and secondary structural building units [38,39]. Possibly, self-assembly of preformed aluminosilicate nanoclusters with the templating micelle will form ordered mesoporous aluminosilicates with strong acidity and high hydrothermal stability.

There are several successful examples for the self-assembly of preformed aluminosilicate nanoclusters with surfactant micelle [40–50], and early works are reported by Pinnavaia *et al*. [40,41] and Xiao *et al*. [42–45].

Pinnavaia *et al* . [40,41] reported that steaming stable mesoporous aluminosilicates with strongly acidic sites are assembled from zeolite seeds solution that normally nucleates the crystallization of microporous zeolites. Assembling these zeolite seeds into a mesostructure imparts acidity and hydrothermal stability that begin to approach zeolites, even though the framework walls remain atomically disordered.

The hexagonal mesoporous aluminosilicates (MSU-S) have been synthesized from zeolite seeds of faujasitic type Y [40], followed by synthesis from zeolite seeds solution of ZSM-5 and Beta in alkaline media [41]. Both XRD and nitrogen adsorption isotherms shows that the mesoporous materials of MSU-S are hydrothermally stable. Catalytic tests in cumene cracking show that MSU-S is much more active than conventional mesoporous aluminosilicates, indicating that the acidic strength of MSU-S is greatly enhanced, as compared with that of MCM-41.

Xiao *et al*. [42,43] reported that ordered hexagonal mesoporous aluminosilicates (MAS-5) with uniform pore sizes have been successfully synthesized from assembly of preformed aluminosilicate precursors with cetyltrimethylammonium bromide (CTAB) surfactant. The aluminosilicate precursors were obtained by heating at 100–140 °C for 2–10 h from alumina–silica gels at the $Al_2O_3/SiO_2/TEAOH/H_2O$ molar ratios of 1.0/7.0–350/10.0–33.0/500–2000.

The small-angle X-ray diffraction pattern for a typical as-synthesized MAS-5 sample shows four well-resolved peaks that can be indexed as (100), (110), (200), and (210) reflections associated with the hexagonal symmetry. No diffraction peak was observed in the region of higher angles 10–40°, which indicates the absence of large microporous crystals in the sample, suggesting that MAS-5 sample is a pure phase.

After calcination in air at 550 °C for 4 h, the sample's XRD pattern shows that the four diffraction peaks are still present, confirming that hexagonal MAS-5 is thermally stable. A similarly high degree of mesoscopic order is observed for hexagonal MAS-5 even after calcination to 900 °C. Interestingly, after treatment of the calcined sample in boiling water for more than 300 h or at 800 °C for 2 h in flowing water steam, the XRD patterns still show those peaks assigned to the hexagonal symmetry, suggesting that the MAS-5 sample has a remarkable hydrothermal stability even at high temperatures.

The acidity of MAS-5 sample was characterized by temperature-programmed-desorption of ammonia (NH_3-TPD) and infrared spectroscopy of adsorbed pyridine. Figure 3 shows NH_3-TPD curves measured on MAS-5, MCM-41, H-ZSM-5, and H-Beta at similar SiO_2/Al_2O_3 ratios (78–84) . Apparently, the desorption temperature of ammonia on MAS-5 is about 410 °C, which is much higher than that of MCM-41 (320 °C) with similar SiO_2/Al_2O_3 ratio. These results indicate that the acidic strength of MAS-5 is much higher than that of MCM-41 and is comparable to that of microporous Beta zeolite.

In catalytic cracking of 1,3,5-triisopropylbenzene, MAS-5 exhibits greater catalytic activity, as compared with MCM-41 and HZSM-5 (table 3). In catalytic alkylation of isobutane with butene, MAS-5 exhibits higher activity than that of calcined MCM-41 with similar SiO_2/Al_2O_3 ratio, which is attributed to strong acidic sites of MAS-5. Furthermore, MAS-5 shows longest catalytic life in all catalysts [42,43], which is assigned to relative low coke formation.

The MAS-5 samples were characterized with infrared, UV-Raman, and NMR spectroscopy and numerous other techniques [42,43]. The results suggest that the pore walls of MAS-5 contains primary and secondary structural building units, similar to those of microporous zeolites [42,43]. Such unique structural features might be responsible for the observed strong acidity and high thermal stability of the mesoporous aluminosilicates with ordered hexagonal symmetry [42,43].

The aluminosilicate precursors were prepared from heating aluminosilicate gel in the presence of TEAOH at 100–140 °C for 2–3 h. TEAOH is known to be a very good structure-directing agent in the synthesis of Beta zeolite [39]. Addition of a small amount of aluminosilicate precursors (3 wt%) into alumina–silica gel ($Al_2O_3/SiO_2/Na_2O/H_2O = 1/10–40/2.8–12/500–900$) at 140 °C for 2–4 days leads to Beta zeolite with high crystallinity in the absence of organic templates [39]. The aluminosilicate precursors appear to serve as seeds for the formation of Beta zeolite. IR characterization of these aluminosilicate precursors shows a clear band at 520–600 cm^{-1}, which is characteristic of 5-membered rings, indicating that aluminosilicate precursors contain zeolite primary and secondary structure building units [51,52].

Table 4 presents textural properties of MAS-5 prepared from preformed Beta zeolite precursors and conventional MCM-41. Interestingly, the thickness of mesoporous walls of MAS-5 is much thicker than that of MCM-41, which is assigned that since the aluminosilicate precursors contain zeolite primary and secondary structure building units, the size of aluminosilicate precursor particles (or nanoclusters) should be larger than that of SiO_4 or $A1O_4$ tetrahedron for constructing the walls of mesopores.

More recently, the assembly of preformed zeolite precursors with surfactants in basic media is applied to synthesize cubic mesoporous aluminosilicates, and NH_3-TPD measurements also show that these samples have similar acidic strength to that of corresponding zeolites [46–49]. Furthermore, the preformed zeolite precursors are extended to zeolite MFI and L nanoclusters [50]. All of these mesoporous aluminosilicates prepared from preformed zeolite nanoclusters with primary and

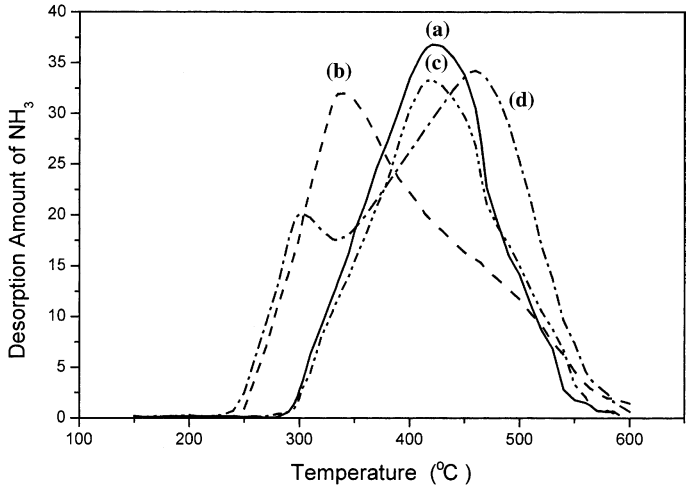

Figure 3. Temperature-programmed-desorption of ammonia (NH_3-TPD) curves for various samples of (a) MAS-5 (b) MCM-41 (c) HBeta and (d) HZSM-5. Reprinted with permission from Ref [89]. Copyright 2001, Wiley.

Table 3
Catalytic activities in cracking of 1,3,5-triisopropylbenzene on various mesoporous aluminosilicate catalysts [42,43]

Sample	SiO_2/Al_2O_3	Treatment	Conversion (%)	Reaction temperature (°C)
HZSM-5	84	–	1.7	250
HMCM-41	80	–	65.8	250
HMCM-41	80	Treated with 100% water vapor at 600 °C for 2 h	< 1.0	250
MAS-5	81	–	78.8	250
MAS-5	81	Boiling water for 300 h	79.1	250
MAS-5	81	Treated with 100% water vapor at 600 °C for 4 h	78.9	250
MAS-5	80	Treated with 100% water vapor at 800 °C for 2 h	77.5	250
MAS-5	123	–	87.0	320
MAS-5	81	–	90.1	320
MAS-5	59	–	95.2	320

Catalytic reactions were performed by pulse injections, and the data presented in this table are the average values of injections. In each run, 50 mg of catalyst was used, pulse injection of the reactant was 0.4 μL, and reaction flow rate was 53.7 mL/min.

secondary building units exhibit much higher hydrothermal stability and acidity than those of conventional MCM-41. Moreover, the acidic strength of ordered mesoporous aluminosilicates could be tailored by using various types of preformed aluminosilicate zeolite nanoclusters, because different types of aluminosilicate zeolites exhibit distinguishable acidic strength [50].

5. Strongly acidic and hydrothermal stable mesoporous aluminosilicates synthesized in strongly acidic media

It is well known that both microporous crystals of zeolites and mesoporous materials are easily synthesized in alkaline media. If the conditions were not controlled very well, mixed phases would often be obtained. On the other hand, in strongly acidic media, the preformed zeolite nanoclusters would not grow continuously into large crystals and the appearance of metal oxides can also be avoided. The products therefore would be pure mesoporous materials without zeolite crystals or metal oxides as by-products.

Table 4
Textural properties for mesoporous aluminosilicate of MAS-5 prepared from preformed Beta zeolite precursors [42,43]

Sample	Unit cell dimension a_0 (Å)	Surface area (m^2/g)	Pore volume (cm^3/g)	Pore size (Å)	Thickness of mesoporous wall (Å)
MAS-5	52.1	1150	1.17	28.1	24.0
MCM-41	44.4	940	0.68	27.9	16.5

The first example for preparation of ordered mesoporous aluminosilicates assembled from preformed zeolite Beta precursors in strongly acidic media is reported by Xiao *et al.* [53]. They reported that heteroatoms of Al are effectively introduced into ordered mesoporous silica materials (MAS-7) by assembly of preformed zeolite Beta nanoclusters with a block copolymer surfactant (P 123) in strongly acidic media (pH < 0) by a two-step procedure. First, preformed zeolite precursors containing zeolite primary and secondary building units were prepared. Secondly, the preformed zeolite precursors were assembled with a polymer surfactant in strongly acidic media. In this way, aluminum species were fixed in the framework of the preformed zeolite nanoclusters in the first step and then directly introduced into the mesoporous walls along with the preformed zeolite nanoclusters in the second step. The most significant advantage of this method is that the Al species in the mesostructure are mostly located at zeolite-like sites, which give the products very high catalytic activity.

Characterization of nitrogen adsorption isotherms and TEM shows that the mesoporous wall (4–5 nm) of MAS-7 is much thicker than that of SBA-15, which is enough for assembly of preformed zeolite precursors (2–3 nm). Recently, Pinnavaia *et al.* [54] reported the assembly of hydrothermally stable and strongly acidic aluminosilicate foams and large-pore hexagonal mesostructures from zeolite seeds under strongly acidic conditions.

Catalytic activities in cracking of cumene and 1,3,5-triisopropylbenzene over various catalysts are summarized in table 5. Although HZSM-5 show strong acidity and give very high conversion for cumene, it is almost inactive for 1,2,3-triisopropylbenzene due to its relative small pore size and the large diameter of reactant molecules. At the same conditions, Al-SBA-15 [55,56] prepared from both "post-synthesis" and "direct synthesis" show relatively low activity, as a result of the amorphous nature of the Al species. Only MAS-7 shows the highest activities for both reactions because it combine the advantages of both zeolite Beta (strong acidity) and SBA-15 (large pores).

Assembly of preformed zeolite ZSM-5 nanoclusters with polymer surfactant (P123) forms ordered mesoporous aluminosilicate (MAS-9) [57]. The XRD pattern and TEM image of the MAS-9 sample shows that MAS-9 has ordered hexagonal arrays of mesopores with uniform size. Combining with the results of N_2 adsorption/desorption experiments which show they have almost the same pore size distributions (80 and 76 Å, respectively), we can conclude that the mesoporous walls of the MAS-9 sample are 20 Å thicker than those of the SBA-15 sample prepared under the same conditions (table 5). This

Table 5
Properties and catalytic activities in cracking of cumene and 1,3,5-triisopropylbenzene (TIPB) of various samples before and after treated in boiling water for 120 h [53,57][a]

Sample	*d*(100) (Å)	Pore size (Å)	Wall thickness (Å)	Micropore volume (cm^3/g)	Surf. area (m^2/g)	Conv. of cumene (%)	Conv. of TIPB (%)
MAS-7	112	76	54	0.15	890	43.5	96.6
MAS-9	116	80	54	0.16	967	41.5	92.4
treated	121	96	43	0.08	680	12.7	34.6
SBA-15	95	76	34	0.05	910	Inactive	Inactive
treated	–	–	–	0	98	Inactive	Inactive
Al-SBA-15	–	–	–	–	924	7.8	36.5
treated	–	–	–	–	85	< 2.0	< 5.0
A1-SBA-15	–	–	–	–	1025	25.5	52.4
treated	–	–	–	–	167	< 2.0	< 5.0
H-ZSM-5	–	–	–	–	–	94.4	1.7

[a]The Si/Al ratio in all samples is 40 except for SBA-15 (pure silica).

phenomenon is assigned to that the nanoclustered MFI primary units used in the synthesis of the MAS-9 have stronger rigidity and larger volume than those non-structured silicon species used in conventional synthesis of SBA-15, therefore the assembly of these nanoclusters needs more space to connect to each other.

Notably, the results of XRD and isotherms for N_2 adsorption (table 5) clearly indicate that the MAS-9 retains an ordered hexagonal structure with surface area of 680 m^2/g even after treatment in boiling water for l20 h. In comparison, SBA-15 and Al-SBA-l5 prepared by conventional method lose most of their mesostructure by the same treatment and retained a surface area less than 200 m^2/g. These results indicate that MAS-9 has much higher hydrothermal stability than SBA-15 and Al-SBA-15.

Catalytic activities in cracking of cumene and 1,3, 5-triisopropylbenzene (TIPB) also show MAS-9 sample is very active for catalytic conversion of both small (cumene) and bulky (1,3,5-triisopropylbenzene) molecules.

Mesoporous aluminosilicates assembled from preformed zeolite precursors in strongly acidic media show large amount of micropores, which are well-characterized by nitrogen adsorption isotherms [53], HR TEM technique [53], probing catalytic reactions [58], and ^{129}Xe NMR spectroscopy [59].

Figure 4 shows the *t*-plots of MAS-7 and SBA-15. Generally, the *t*-plots of conventional mesoporous materials should pass zero of axis, which means there is no micropores in them. Miyazawa *et al*. reported that there are some micropores in the wall of SBA-15 formed by penetration of hydrophilic poly (ethylene oxide) chains of triblock coplymer in the silica wall [60]. The SBA-15 sample also shows the evidence of containing micropores. However, it is very interesting to note that the micropore volume of both MAS-7 and MAS-9 samples (0.15 and 0.16 cm^3 /g) is much more than that of the SBA-15 sample prepared under the same conditions (0.05 cm^3/g). Even we considered the fact that MAS-7 and MAS-9 samples have thicker walls than SBA-15, the ratio of micropores volume to the thickness of the walls in MAS-9 is still much more than that in SBA-15. The larger micropore volume in MAS-7 and MAS-9 may be attributed to the existence of zeolite primary units in the mesoporous walls [61].

Figure 5 shows the TEM image of MAS-7 viewed down the (100) and (110) direction. Clearly, the TEM image of MAS-7 recorded along the (110) shows obvious white dots of 7 Å except for the mesopores (pore size of 7.4 nm), which could possibly be assigned to micropores in the mesoporous walls of MAS-7.

Microporosity of ordered mesoporous aluminosilicates assemblied from zeolite nanoclusters is also investigated by catalytic reactions with various probing molecules [58], including isopropanol dehydration and cracking of cumene and TIPB. The molecular diameter of isopropanol, cumene, TIPB and 5,7-dibromo-8-hydroxy-chinolin (DBHC) is 3.4, 5.0, 7.4, and 8.7 Å, respectively. If the acidic samples are treated by basic molecule of DBHC, the acidic sites in the pores larger than 8.7 Å will be killed, and the acidic sites in the pores less than 8.7 Å will still be active. Then we can test their catalytic activity by using probing molecules smaller than DBHC in order to fudge what kind of micropores these samples contain.

Table 6 presents catalytic activities of various samples without treatment of DBHC. In isopropanol dehydration, ZSM-5, Beta, Al-SBA-15, MAS-7, and MAS-9 show very high activity, giving nearly 100% conversion. In cumene cracking, microporous zeolites of ZSM-5 and Beta exhibit high activity. In contrast, the mesoporous aluminosilicates of Al-SBA-15, MAS-7, and MAS-9 show relatively low conversion. Furthermore, MAS-7 and MAS-9 are more active than Al-SBA-15 with the same Si/Al ratio, indicating that the acidic strengths of MAS-7 and MAS-9 are much stronger than that of Al-SBA-15. In TIPB cracking, the samples of Beta, Al-SBA-15, MAS-7, and MAS-9 show high activity. However, ZSM-5 shows relatively low

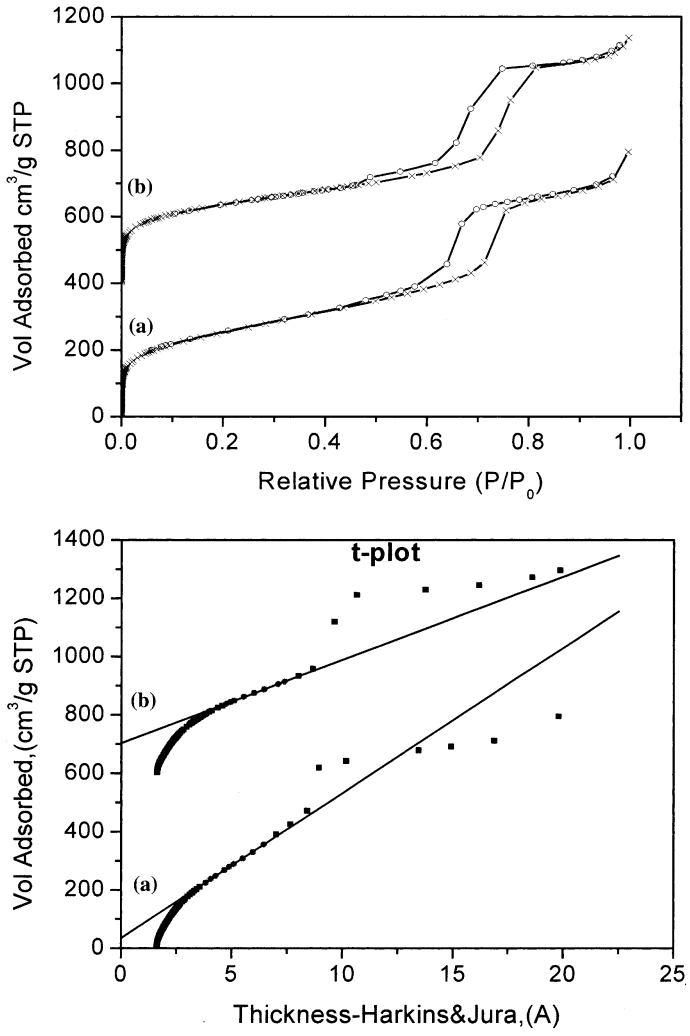

Figure 4. N_2 adsorption/desorption isothems (top) and *t*-plots (bottom) for calcined: (a) SBA-15 and (b) MAS-7. The isotherm and *t*-plot for B are, respectively, offset between 400 and 600 cm^3/g to begin for clarity.

catalytic activity, which is assigned that the reactant molecule of TIPB cannot enter the pores of ZSM-5.

Table 7 presents catalytic activities of various samples treated by DBHC. In catalytic cracking of large molecule of TIPB, the treated Al-SBA-15 samples are inactive, suggesting that the acidic sites in the pores larger than 8.7 Å are killed and there are no micropores with size between 7.4 and 8.7 Å. However, the treated MAS-7 still shows a conversion of 12.5%, suggesting that there are micropores with size between 7.4 and 8.7 Å. Considering the pore size of zeolite Beta is about 7.7 Å, we propose that the microporosity with size between 7.4 and 8.7 Å is introduced by preformed zeolite Beta nanoclusters used in the synthesis. Additionally, we find that the treated MAS-9 is also inactive, suggesting that there are no micropores with size between 7.4 and 8.7 Å.

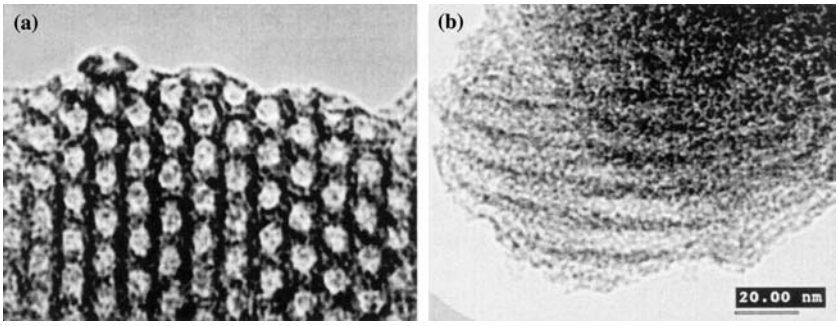

Figure 5. TEM image of MAS-7: (a) in the direction of the pore axis (100) and (b) in the direction perpendicular to the pore axis (110).

Table 6
Catalytic activities of various samples without treatment of DBHC molecules [58]

Catalyst (Si/Al)	Conversion (%)		
	Isopropanol dehydration	Cumene cracking	1,3,5-triisopropylbenzene (TIPB) cracking
ZSM-5 (30)	100	90.1	4.5
Beta (30)	100	93.4	100
Al-SBA-15 (30)	100	12.5	92.5
Al-SBA-15 (20)	100	33.2	98.4
MAS-7 (30)	100	30.4	97.3
MAS-9 (30)	100	29.5	95.1

In catalytic cracking of small cumene molecule, the treated Al-SBA-15 samples are inactive. Considering the fact the acidic sites in the pores larger than 8.7 Å are killed by DBHC molecule, it is suggested that there are no micropores with size between 5.0 and 8.7 Å in Al-SBA-15. However, the treated MAS-7 and MAS-9 samples show conversion at 3.5 and 3.2%, respectively, suggesting that the two samples contain micropores with size between 5.0 and 8.7 Å. As MAS-9 is inactive for TIPB cracking, we conclude that the microporous size of MAS-9 should be 5.0–7.4 Å, in consistent with the pore size (5.4 × 5.5 Å) of ZSM-5 zeolite.

In catalytic dehydration of isopropanol, the treated mesoporous aluminosilicates of Al-SBA-15, MAS-7, and MAS-9 also show high activity, indicating that these mesoporous aluminosilicates contain micropores in the range of 3.4–8.7 Å. By considering the fact the treated Al-SBA-15 is completely inactive for cumene and TIPB cracking, it is suggested that the microporous size in Al-SBA-15 is 3.4–5.0 Å, which is in good agreement with early literature [60].

^{129}Xe NMR spectroscopy is an important and very useful technique for investigating the pore structure of porous materials [62,63]. ^{129}Xe is an inert, nonpolar, spherical atom with a large electron cloud sensitive to its environment and interactions, which results in a wide ^{129}Xe NMR chemical shift range. Together with a nuclear spin 1/2 and a relatively high NMR sensitivity, ^{129} Xe is as an ideal NMR probe.

The ^{129}Xe NMR spectra of xenon adsorbed in MAS-7 with an adsorption pressure of xenon varying from 4.66×10^3 to 2.5×10^6 Pa show two well-resolved resonances at about 75 and 53 ppm at room temperature, while only a single resonance is present in the ^{129}Xe NMR spectra of SBA-15 and MCM-41 within a large range of xenon pressure [59]. The chemical shifts of the two signals following a parabolic correlation against the adsorption pressure of xenon should arise from the presence of micropores as strong adsorption sites in the mesoporous MAS-7 [64]. Obviously, the variations of the chemical shift and the integrated intensities of the two signals is quite different from those for the line *a* and line *b* observed in the ^{129}Xe NMR spectra of MAS-7. Therefore, we incline to assign the two signals in the ^{129}Xe NMR spectra of MAS-7 to xenon adsorbed in two types of micropores rather than xenon in micropores and mesopores, respectively. We denote the micropores corresponding to line *a* and line *b* as "micropore I" and "micropore II", respectively. Xenon atoms in the two types of micropores may probably undergo fast exchange with those in the void of mesoporoes. However, they exchange slowly between themselves within NMR time scale. The chemical shifts of the two signals are an average of the shifts of xenon in the micropores and mesopores of MAS-7. The observation of two separate resonances over a wide range of xenon pressure also suggests that there is no direct communication between the two different types of micropores. That is to say, they are independent pore systems.

Adsorption of different sizes of guest molecules in microporous materials is a conventional technique for estimating the micropore sizes. Small molecules preferentially trapped in micropores can reduce the proportion of xenon in these pores, which will lead to a decrease in the observed ^{129}Xe NMR chemical shift. To confirm this assumption, several guest molecules with different sizes are adsorbed in MAS-7. After co-adsorption of xenon and water molecule in MAS-7, a significant decrease (ca. 25 ppm) in the ^{129}Xe chemical shift of the two signals is observed in the hydrated sample of MAS-7, which depends on the loading of water molecules.

After co-adsorption of xenon and benzene (with a kinetic diameter of 0.49 nm) [65], the ^{129}Xe NMR chemical shift of the down-field signal is decreased by ca. 10 ppm while that of the up-field signal remains almost unchanged, indicating that benzene molecules can penetrate into micropore I, while micropore II is not accessible to benzene molecules. In the case of co-adsorption of xenon and 1,3,5-triisopropylbenzene (TIPB) (with a kinetic diameter 0.74 nm) [65], we observed a much smaller decrease (ca. 3 ppm) in the chemical shift of the down-field signal and a decrease in the integrated intensity of up-field signal, suggesting that only small amount of

Table 7
Catalytic activities of various samples with treatment of DBHC molecules [58]

Catalyst (Si/Al)	Conversion (%)		
	Isopropanol dehydration	Cumene cracking	1,3,5-triisopropylbenzene cracking
ZSM-5 (30)	100	89.2	–
Beta (30)	100	92.7	100
Al-SBA-15 (30)	41.1	–	–
Al-SBA-15 (20)	100	–	–
MAS-7 (30)	81.1	3.5	12.5
MAS-9 (30)	79.2	3.5.	–

–, Undetectable.

TIPB molecules can get into micropore I while micropore II is not accessible to TIPB. Based on the co-adsorption experiments, it can be estimated that the size of micropore I assigned to preformed zeolite Beta nanoclusters is close to 0.74 nm, and that of micropore II assigned to partial occlusion of triblock polymer chains into the mesoporous walls is in the range of 0.44–0.49 nm, which is in good agreement with those investigated by nigrogen adsorption, TEM, and catalytic probing molecules [58].

As revealed by our ^{129}Xe NMR experiments, although no direct communication is present between the two different types of micropores, there is a good communication between the two different types of micropores and the mesopores in MAS-7. In addition, two neighboring mesopores are interconnected through the micropores. For example, the small molecules (such as xenon and water) adsorbed in one mesopore can pass through the pore wall that contains the two types of micropores to another neighboring mesopore. We suspect that the good communication network formed inside MAS-7 should be crucial to its excellent catalytic performance.

The preformed zeolite nanoclusters in ordered mesoporous aluminosilicates are also measured with HR TEM [66], and obtained results in TEM images showed ordered arrays at around 2– 3 nm in size, which is very similar to the size of preformed zeolite nanoclusters reported previously [67]. This conformed that the mesoporous walls are partially polycrystallized although the size is relatively small (around 2–3 nm).

6. Hydrothermal stable mesoporous titanosilicates with catalytically active titanium species in oxidations

There is currently great interest in titanium-containing zeolitic catalysts for selective oxidation. Since the discovery of microporous TS-1 by Enichem Company [68], a series of microporous titanosilicates, Ti-ZSM-12 [69], Ti-ZSM-48 [70], and Ti-Beta [71], have been reported which have remarkable catalytic properties [68–73]. However, one disadvantage of these titanosilicate catalysts is that their pores are too small for access by bulky reactants of the kind important in fine chemical and pharamaceutical industries. Recent progress in solving this has been the incorporation of titanium ions into the framework of mesoporous materials (MCM-41, HMS and SBA-15) [74–19] and the grafting of a titanocene complex onto mesoporous silica [80]. These mesoporous titanosilicate materials have pore diameters of 30–60 Å and exhibit catalytic properties for the oxidation of bulky reactants under mild conditions, but unfortunately, when compared with TS-1 and Ti-Beta, the oxidation ability and hydrothermal stability are relatively low, which severely hinders their practical applications. The relatively low oxidiation ability and hydrothermal stability, e.g. of Ti-MCM-41, can be attributed to the difference in the titanium coordination environment (amorphous nature of the mesoporous wall) [2]. Recently, there had been great progress in the preparation of mesostructured materials assembled from nanoclusters, such as mesostructured metal germanium sulphides [81] and mesoporous aluminosilicate nanoclusters [41–43].

We show here that through the assembly of preformed titanosilicate precursors [82] with triblock copolymers in a strongly acidic media an ordered mesoporous titanosilicate (MTS-9) that is hydrothermally stable can be synthesized [83,84]. Catalytic tests show that MTS-9 is very active for the oxidation of the smaller molecules of phenol and styrene and also of the bulky molecule of trimethylphenol.

XRD and TEM imaging clearly indicate that MTS-9 has ordered hexagonal arrays of mesopores with uniform size. Notably, after treatment of MTS-9 in boiling water for over 120 h, the XRD patterns still show the peaks assigned to hexagonal symmetry, showing that MTS-9 is extremely hydrothermally stable, as compared to Ti-MCM-41 and SBA-15. Additionally, the d(l00) value of MTS-9 is much larger than that of SBA-15 prepared under the same condition. The measurement of their N_2 isotherms shows that these two samples have almost the same pore size, which means that the pore wall of MTS-9 is much thicker than that of SBA-15.

Catalytic activities for the oxidation of aromatics by H_2O_2 over MTS-9, Ti-MCM-41, and TS-1 catalysts are presented in table 8. In phenol hydroxylation, Ti-MCM-41 shows very low catalytic activity, but MTS-9 exhibits very high catalytic activity, with a phenol conversion of 26% which is comparable with TS-1[68]. In 2,3,6-trimethylphenol hydroxylation, Ti-MCM-41 is inactive due to the relatively low oxidation ability of Ti species in the amorphous wall of Ti-MCM-41, and TS-1 is also inactive due to the inaccessibility of the small micropores of TS-1 to the large diameter of a bulky molecule like 2,3,6-trimethylphenol. However, MTS-9 is very active for this reaction with a conversion of 18.8% indicating that MTS-9 is an effective catalyst for the oxidation of bulky molecules.

The catalytically active Ti species in MTS-9 have been characterized by UV–visible and UV–Raman techniques. The U V–vis spectrum for MTS-9 has an adsorption band near 215 nm, which is very similar to TS-1. This indicates that the coordination environment of the Ti species in MTS-9 is similar to that in TS-1. In contrast, Ti-MCM-41 shows maximum adsorption at 230 nm, which had been assigned to titanium with a coordination number between 4 and 6 [74]. Furthermore, UV–Raman spectroscopy shows that MTS-9 exhibits a band at 1122 cm^{-1} , which is very close to that band of TS-1(1125 cm^{-1}) [85], demonstrating 4-coordinated Ti species in MTS-9.

We proposed that the good hydrothermal stability and high catalytic activity of MTS-9 are due to the TS-1-like coordination enviroment of the Ti species in the mesoporous wall containing the zeolite primary and secondary building units (PSBU). The evidence for this is also

Table 8
Catalytic activities in oxidation reactions by H_2O_2 over MTS-9, Ti-MCM-41, and TS-1 samples [83]

Samples	Reactions	TOF	Conv. (%)	Product selectivity, (%)		
				P1	P2	P3
MTS-9	Phenol hydroxylation[a]	6.8	26.3	59.5	39.8	0.7
Ti-MCM-41	Phenol hydroxylation[a]	0.5	2.5	60.1	38.0	1.9
Ti-HMS[b]	Phenol hydroxylation[a]	0.1	0.5	58.5	41.5	0.5
TS-1[c]	Phenol hydroxylation[a]	5.5	28.0	50.4	48.6	1.0
MTS-9	Styrene epoxidation[d]	9.4	56.4	28.0	29.3	42.7
Ti-MCM-41	Styrene epoxidation[d]	6.1	48.3	–	–	100
TS-1[c]	Styrene epoxidation[d]	5.2	54.6	13.3	58.3	29.0
MTS-9	Trimethylphenol hydroxylation[e]	7.4	18.8	66.7	21.1	12.2
Ti-MCM-41	Trimethylphenol hydroxylation[e]	1.4	4.1	25.5	69.8	4.6
Ti-HMS[b]	Trimethylphenol hydroxylation[e]	0.5	2.0	25.0	70.0	5.0
TS-1[c]	Trimethylphenol hydroxylation[e]	0.3	1.2	71.1	17.6	11.3

[a]Reaction conditions: water as a solvent, reaction temperature at 80 °C, phenol/H_2O_2 = 3/1 (molar ratio), reaction time for 4 h, catalyst/phenol = 5% (weight ratio). The products are catechol (P1), hydroquinone (P2), and benzoquinone (P3). The product of tar is not included.
[b]Ti-HMS with Si/Ti ratio of 30.
[c]Ts-1 with Si/Ti ratio of 30.
[d]Reaction conditions: Aceton as a solvent, reaction temperature at 45 °C styrene/H_2O_2 = 3/1(molar ratio), reaction time for 5 h, catalyst/phenol = 5% (weight ratio). The products are styrene epoxide (P1), phenylacetaldehyde (P2), and benzaldehyde (P3).
[e]Reaction conditions: Acetonitrile as a solvent, reaction temperature at 80 °C, trimethylphenol/H_2O_2 = 3/1(molar ratio), reaction time for 4 h, catalyst/phenol = 5% (weight ratio). The product are trimethylhydroquinone (P1), trimethylbenzoquinone (P2), others (P3).

provided by IR spectroscopy. The spectrum of MTS-9 gives the band at 550 cm^{-1} which is characteristic of 5-rings of PSBU in TS-1 zeolite [51,52]. In contrast, we cannot detect this band with Ti-MCM-41.

We proposed that during the preparation of MTS-9 the titanium sites are fixed in the framework of the TS-1 nanoclusters in the first step and are introduced into the mesoporous structure when the nanoclusters self-assemble with the template in the second step. Since TS-1 nanoclusters (primary and secondary structure building units) are more rigid and have a larger volume in the synthesis of MTS-9 as.compared with non-structured silicon in the synthesis of SBA-15, the assembly of these titanosilicate nanoclusters needs more space to join with each other, and this results in the walls in MTS-9 being thicker than that in SBA-15 (table 1).

Recently, the self-assembly of preformed zeolite TS-1 nanoclusters with surfactant micelle is extended to alkaline conditions by using CTAB [86], and the obtained ordered mesoporous titanosilicates also exhibit high catalytic activities in oxidations with hydrogen peroxide, and characterization of UV–visible spectroscopy also show that the titanium sites in these mesoporous titanosilicates are TS-1-like [86].

7. High-temperature generalized syntheses of ultrastable ordered mesoporous silica-based materials by fluorocarbon–hydrocarbon surfactant mixtures

A number of successful examples of mesoporous materials with good hydrothermal stability have been reported recently [40– 43], but their hydrothermal stability is still much lower than that of zeolites, which severely hinders their practical applications in catalytic reactions for petroleum industry. For example, FCC catalysts need to be hydrothermally stable in 100% steaming at 80 °C for 5 h at least, which is also the lowest requirement for FCC zeolite catalysts [87].

On the other hand, it is interesting to note that the mesostructured materials are prepared at room temperature or relatively low temperatures (80–150 °C). This is quite different from the higher temperatures (150–220 °C) used for the syntheses of many microporous zeolites or phosphates, and it is because surfactant molecules will not be able to direct mesoporous structure formation due to unfavorable conditions for micelle formation at the higher temperatures [88]. In some cases, the large-chain surfactants will even decompose above 150 °C.

However, for silica-based materials, a critical factor in increasing hydrothermal stability is to have more silica condensation on the pore walls [89], but low synthetic temperatures result in imperfectly condensed mesoporous walls with large amounts of terminal hydroxyl groups which make the mesostructure unstable [1]. Possibly, the level of silica condensation will be enhanced by increasing the crystallization temperature. Therefore, high-temperature synthesis of mesoporous materials is attractive.

Unfortunately, there is no surfactant that can be used as template at high temperature. Fluorocarbon surfactants are a kind of stable surfactants which are widely used at high temperatures (> 200 °C) [90]. However, due to the rigidity and strong hydrophobicity of the fluorocarbon chains [90], fluorocarbon surfactants cannot be formed ordered surfactant micelle, and therefore these

fluorocarbon surfactants are not suitable as templates for the preparation of well-ordered mesoporous materials. Recently, there are successful examples to form ordered surfactant micelle by mixing nonionic surfactants with ionic surfactants [91,92]. Hopefully, the mixture of an ordered polymer surfactant micelle with a stable fluorocarbon surfactant could form an ordered and stable surfactant mixture micelle at high temperature (>150 °C).

Fortunately, according to this idea, the ordered and stable surfactant mixture micelle at high temperature is successfully prepared by the mixture of P123 with FC-4 ($C_3F_7O(CFCF_3CF_2O)_2CFCF_3CONH(CH_2)_3N^+(C_2H_5)_2CH_3I^-$). When this mixture is used as the template, highly ordered mesoporous silica-based materials with unusual hydrothermal stability, designated JLU-20, are effectively synthesized in strong acidic media at high temperatures (160–220 °C) [93].

In a typical synthesis, 1.2 g of FC-4 and 0.4 g of P123 were dissolved in 20 mL of H_2O with 5 mL of HCl (10 M/L), followed by 2.4 mL of tetraethyl orthosilicate (TEOS). After stirring at 40 °C for 20 h, the mixture was transferred into an autoclave for further condensation at 190 °C for 4 h. The product was collected by filtration, dried in air and calcined at 650 °C for 5 h to remove the surfactant template. The product is named JLU-20.

The X-ray diffraction (XRD) pattern of calcined JLU-20 (figure 6b) shows four clearly well-resolved peaks that can be indexed as the (100), (110), (200), (210) diffractions associated with the *P6mm* hexagonal symmetry with a lattice constant $a = 118$ Å. In contrast, ordered mesostructured silica cannot be formed via a high temperature crystallization in the absence of FC-4 (figure 6d). Notably, JLU-20 is much more hydrothermally stable than SBA-15.[3] Upon hydrothermal treatment, JLU-20 remains well-ordered (figure 6c), whereas SBA-15 loses most of its mesostructure (table 9). Figure 6a and 6b shows that the unit cell of JLU-20 does not contract during calcination at 650 °C for 2 h and demonstrates its excellent thermal stability (table 9).

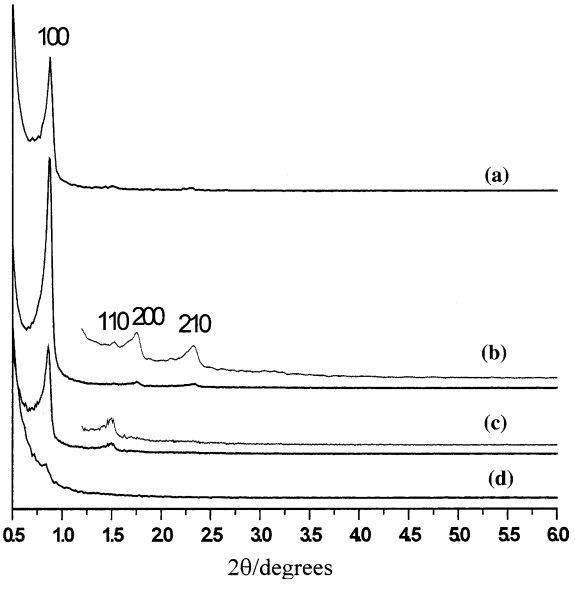

Figure 6. XRD patterns of as-synthesized JLU-20 (curve a), calcined JLU-20 (b), JLU-20 treated in boiling water for 8 h (c) and as-synthesized sample prepared with the same procedure as JLU-20 except for the absence of FC-4 in the initial reaction mixture (d). Reprinted with permission from Ref [89]. Copyright 2003, Wiley.

TEM images of calcined JLU-20 show well-ordered hexagonal arrays of mesopores with one-dimensional channels and further confirm that JLU-20 has a two-dimensional hexagonal *(P6mm)* mesostructure. Interestingly, JLU-20 has continuous zigzag mesoporous channels which can be as long as 6 μm [93], much longer than those in conventional SBA-15 [3]. Such continuous ultra-long channels have not been reported before. Additionally, during observations by TEM, unlike most ordered mesoporous materials that are extremely vulnerable to heating and electron radiation, JLU-20 is not damaged even under relatively strong current density for a long time. This is another indication that JLU-20 possesses unusual stability.

The ^{29}Si MAS NMR spectrum of the as-synthesized JLU-20 provides direct evidence of the extent of silica condensation. JLU-20 is primarily made up of fully condensed Q^4 silica units (−112 ppm) with a small contribution from incompletely cross-linked Q^3 (−102 ppm), giving very high Q^4/Q^3 ratio (6.5). In contrast, SBA-15 has typical peaks correspond to Q^2, Q^3, and Q^4 silica species respectively, and the ratio of Q^4/Q^3+Q^2 is 1.9 (table 9), suggesting the presence of large amounts of terminal hydroxyl group in the framework. Obviously, JLU-20 has fully condensed mesoporous silica walls.

The N_2 adsorption isotherms (table 9) further indicate the ultra high stability of JLU-20. For example, after hydrothermal treatment in boiling water for 120 h, there is only a decrease in BET surface area of 7% for JLU-20 whereas it is 68% for SBA-15. Furthermore, the isotherm of the treated JLU-20 sample is still a typical IV isotherm, implying the good maintenance of the uniform mesopores. Its pore size distribution curve is as sharp as the untreated sample. In contrast, the treated SBA-15 shows a poor isotherm with an undiscernible pore size distribution.

It is worth noting that as-synthesized JLU-20 has a relatively low surface area (300 m^2/g) and pore volume (0.46 cm^3/g) when compared with SBA-15. However, JLU-20 strictly fulfills the fundamental relation between the structural parameters for materials with uniform pores of simple cylindrical geometry: $wS/V \approx 4$ (w, S, and V denote pore size, surface area and pore volume, respectively) [94]. This suggests that JLU-20 is free of micropores in the mesoporous walls which is confirmed by N_2 adsorption isotherm *t*-plots.

The fully silica condensation and high stability of JLU-20 should be attributed directly to the

Table 9
Properties of the samples before and after hydrothermal and steaming treatment [93][a]

Sample	d(100) (Å)	Pore size (Å)	Wall thickness (Å)	Pore volume (cm^3/g)[b]	Surface area (m^2/g)	Q^4/Q^3+Q^2	wS/V
JLU-20	101					6.5	
Calcined	101	62	55	0.46	300		4.0
Treated[c]	101	66	51	0.44	278		4.2
Treated[d]	95	65	45	0.32	225		4.5
SBA-15	110					1.9	
Calcined	105	78	43	1.45	1005		5.4
Treated[c]				1.08	320		
Treated[d]				0.35	214		

[a]Pore size distributions and pore volumes determined from N_2 adsorption isotherms at 77 K and the wall thickness was calculated as: thickness = a-pore size ($a = 2 \times d_{(100)}/3^{1/2}$); In the last column, w, S, and V denote pore size, surface area, and pore volume, respectively; because SBA-15 was rendered amorphous after the hydrothermal or steaming treatment, there are no $d(100)$ values, pore sizes and wall thickness for the treated SBA-15 samples given in this table.
[b]The pore volume here is the primary mesopore volume (BJH adsorption cumulative pore volume of pores between 20 and 250 Å diameter).
[c]Treated in boiling water for 120 h.
[d]Treated with 100% water vapor at 800 °C for 2 h.

high-temperature of the synthesis rather than other reasons such as the fluorocarbon surfactant. If JLU-20 is prepared at 100 °C instead of at 190 °C, it shows no difference in both structural properties (surface area, pore volume, Q^4/Q^3 ratio, etc.) and stability with conventional SBA-15 although FC-4 is used. However, the use of the fluorocarbon surfactant allows full condensation *via* a high-temperature synthesis. This method is not limited to the combination of FC-4 with P123, and many mixtures of hydrocarbon and fluorocarbon surfactants can be used if they effectively form a regular mixed micella in solution with suitable interactions between the chosen surfactant and inorganic species. This method opens the door for the preparation of a series of ordered mesoporous materials with various mesostructures such as two-dimensional hexagonal *P6mm,* cubic *Ia3d,* cubic *Pm3n,* and three-dimensional hexagonal $P6_3$/mmc. For example, mesoporous silica with cubic *Im3m* symmetry (figure 7) has been obtained recently by using the surfactant mixture of FC-4 and triblock copolymer F127 as template and the resulted material is much hydrothermally stable than its counterpoint prepared at low temperature, SBA-16.

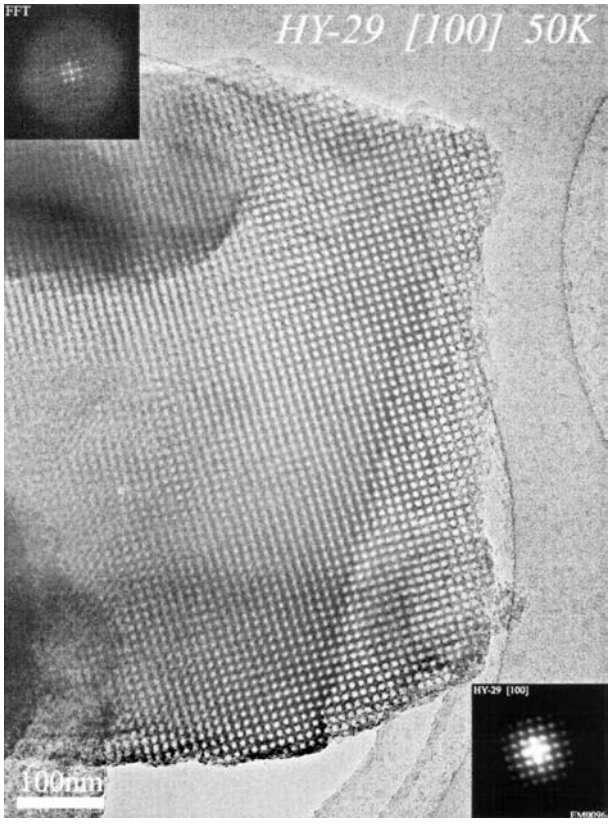

Figure 7. TEM image of calcined JLU-21 taken in the (100) direction (A). Insets are the selected-area ED and FFT patterns of these images. Mesoporous cubic silica was synthesized from the assembly of TEOS with mixture surfactant of F127 and FC-4 at 140–160 °C.

Additionally, we have successfully introduced heteroatoms (active sites in catalysis) such as Al and Ti into the mesoporous wall of JLU-20. Both of these exhibit much higher hydrothermal stabilities than pure silica JLU-20. The detail results will be published in near future.

8. Conclusion

To increase catalytic activity and stability of mesoporous materials, various routes have been employed, which include (1) acidic sulfated zirconia supported into mesoporous materials; (2) strongly acidic and thermally stable mesostructured sulfated zirconia with tetragonal crystalline phase; (3) strongly acidic and hydrothermally stable mesoporous aluminosilicates synthesized in alkaline media; (4) strongly acidic and hydrothermally stable mesoporous aluminosilicates synthesized in strongly acidic media; (5) hydrothermally stable mesoporous titanosilicates with catalytically active titanium species in oxidations; (6) high-temperature generalized synthesis

of stable ordered mesoporous silica-based materials by using fluorocarbon–hydrocarbon surfactant mixtures. Apparently, ordered mesoporous materials with high stability and catalytic activity would be potentially important for the industrial application as versatile catalysts.

Acknowledgments

This work was supported by the National Natural Science Foundation of China, the State Basic Research Project, CNPC, BASF, and the National Advanced Materials Committee of China.

References

[1] C.T. Kresge, M.E. Leonowicz, W.J. Roth, J.C. Vartuli and J.S. Beck, Nature 352 (1992) 710.
[2] A. Corma, Chem. Rev. 97 (1997) 2373.
[3] D. Zhao, J. Feng, Q. Huo, N. Melosh, G.H. Fredrickson, B.F. Chmelka and G.D. Stucky, Science 279 (1998) 548.
[4] S.S. Kim, W. Zhang and T.J. Pinnavaia, Science 282 (1998) 1032.
[5] R. Ryoo, J.M. Kim and C.H. Shin, J. Phys. Chem. 100 (1996) 17718.
[6] R. Ryoo, S. Jun, J.M. Kim and M.J. Jim, Chem. Commun. (1997) 2225.
[7] R. Mokaya and W. Jones, Chem. Commun. (1997) 2185.
[8] R. Mokaya, Angew. Chem. Int. Ed. 38 (1999) 2930.
[9] Q.S. Huo, et al., Nature 368 (1994) 317.
[10] P.D. Yang, D.Y. Zhao, D.I. Margolese, B.F. Chmelka and G.D. Stucky, Nature 396 (1998) 152.
[11] D.M . Antonelli and J.Y. Ying, Curr. Opin. Colloid Interface Sci. 1 (1996) 529.
[12] T. Sun and J.Y. Ying, Nature 389 (1997) 704.
[13] C. Chen, H. Li and M.E. Davis, Microporous Mater. 2 (1993) 17.
[14] D. Khushalani, A. Kuperman, N. Coombs and G.A. Ozin, Chem. Mater. 8 (1996) 2188.
[15] X.S. Zhao and G.Q. Lu, J. Phys. Chem. B 102 (1998) 1556.
[16] J.M. Kim, S. Jun and R. Ryoo, J. Phys. Chem. B 103 (1999) 6200.
[17] K. Arata, Adv. Catal. 37 (1990) 165.
[18] H.-Q. Xia, K. Hidajat and S. Kawi, J. Catal. 205 (2002) 318.
[19] T. Jin, T. Yamaguchi and. K. Tanabe, J. Phys. Chem. 90 (1986) 4797.
[20] M. Hino and K. Arata, Chem. Commun. (1979) 1148.
[21] G.D. Yadav and J.J. Nair, Microporous Mesoporous Mater. 33 (1999) 1.
[22] T. Lei, W.-M. Hua, Y. Tang, Y.-H. Yue and Z. Gao, Chem. J. Chinese Univ. 21 (2000) 1240.
[23] H.-Q. Xia, K. Hidajat and S. Kawi, Chem. Commun. (2000) 2229; M. Matsuhashi, M. Tanaka, H. Nakamura and K. Arata, Appl. Catal. A. 208 (2001) 1.
[24] C.-L. Chen, S. Cheng, H.-P. Lin, S.-T. Wong and C.-Y. Mou, Appl. Catal. A. 215 (2001) 21.
[25] W. Hua, Y. Yue and Z. Gao, J. Mol. Catal. A. 170 (2001) 195.
[26] Y. Sun, L. Zhu, H. Lu, R. Wang, S. Lin, D. Jiang, and F.-S. Xiao, Appl. Catal. A. 237 (2002) 21.
[27] F.-S. Xiao, S. Zheng, J. Sun, R. Yu, S. Qiu and R. Xu, J. Catal. 176 (1998) 474.
[28] Y.Y. Sun, L.-N. Yuan, W. Wang, C.L. Chen and F.-S. Xiao, Catal. Lett. 87 (2003) 57.
[29] X.M. Song and A. Sayari, Catal. Rev. – Sci. Eng. 38 (1996) 329.
[30] X. Yang, F.C. Jentoft, R.E. Jentoft, F. Girgsdies and T. Ressler, Catal. Lett. 81 (2002) 25.
[31] S. Kobayashi and K. Arata, J. Am. Chem. Soc. 101 (1979) 6439.
[32] E.J. Holsten, J.T. Wei and C.-Y. Hsu, U.S. Patent 4918041, 1990.
[33] C.Y. Hsu, C.R. Heimbuch, C.T. Armes and B.C. Gates, Chem. Commun. (1992) 1645.
[34] M.A. Coelho, D.E. Resasco, E.C. Skabwe and R.L. White, Catal. Lett. 32 (1995) 256.
[35] W.-M. Hua, Y.-D. Xia, Y. H. Yue and Z. Gao, J. Catal. 196 (2000) 104.
[36] J.A. Moreno, G. Poncelet, J. Catal. 203 (2001) 453; W. Hua, J. Sommer, Appl. Catal. A. 227 (2002) 279; U. Ciesla, S. Schacht, G.D. Stucky, K.K. Unger and ¸ F. Schuth, Angew. Chem. Int. Ed. 35 (1996) 541.
[37] Y.Y. Sun, L. Yuan, S.Q. Ma, Y. Han, L. Zhao, W. Wang, C.L. Chen and F.-S. Xiao, Appl. Catal. A 268 (2004) 17.
[38] H. Robson, ACS Symp. Ser. 398 (1989) 436.
[39] Q. Zhou, W. Pang, S. Qiu, M. Jia, CN Patent, ZL 93 1 17593.3,1996; Q. Zhou, B. Li, S. Qiu and W. Pang, Chem. J. Chinese Univ. 20 (1999) 693.
[40] Y. Liu, W.Z. Zhang and T.J. Pinnavaia, J. Am. Chem. Soc. 122 (2000) 8791.
[41] Y. Liu, W.Z. Zhan and T.J. Pinnavaia, Angew. Chem. Int. Ed. Engl. 40 (2001) 1255.
[42] Z. Zhang, Y. Han, L. Zhu, R. Wang, Y Yu, S. Qiu, D. Zhao and F.-S. Xiao, Angew. Chem. Int. Ed. Engl. 40 (2001) 1258.
[43] Z. Zhang, Y. Han, F.-S. Xiao, S. Qiu, L. Zhu, R. Wang, B. Zou, H. Sun, Z. Zhang, D. Zhao and W. Yen, J. Am. Chem. Soc. 123 (2001) 5014.
[44] Y. Han, Y. Yu and F.-S. Xiao, Chinese J. Chem. 20 (2002) 711.
[45] F.-S. Xiao, Y. Han and S. Qiu, Chem. J. Chinese Univ. 23 (2002) 1847.
[46]. F.-S. Xiao, Stud. Surf. Sci. Catal. 135 (2001) 06-P-07.
[47] G. Li, Q.-B. Kan, T.-H. Wu, C.-M. Hou, J.-H. Huang, S.-J. Wu and C. Li, Chem. J. Chinese Univ. 23 (2002) 1171.
[48] P.-C. Shih, H.-P. Lin and C.-Y. Mou, Stud. Surf. Sci. Catal. 146 (2003) 557.
[49] J.L. Zheng, Y. Zhang, W. Wei, D. Wu, Y.H. Sun, F. Deng, Q. Luo and Y. Yue, Acta Physico-Chimica Sinica 19 (2003) 907.
[50] Y. Di, Y. Yu, Y.Y. Sun, X.Y. Yang, S. Lin, M.Y. Zhang, S.G. Li and F.-S. Xiao, Microporous Mesoporous Mater. 62 (2003) 221; L. Sen, L.-F. Wang, Y. Han, Y. Yu, D. Yan, R.W. Wang, D.Z. Jiang and F.-S. Xiao, Chinese J. Chem. 22 (2004) 9.
[51] P.E.A. de Moor, T.P.M. Beelen, B.U. Komanschek and R.A. van Santen, Microporous Mesoporous Mater. 21 (1998) 263.
[52] A. Jacobs, E.G. Derouane and J. Weitkamp, Chem. Commun. (1981) 591.
[53] Y. Han, F.-S. Xiao, W. Wu, Y. Sun, X. Meng, D. Li, S. Lin, F. Deng and X. Ai, J. Phys. Chem. B 105 (2001) 7963.
[54] Y. Liu, T.J. Pinnavaia, Chem. Mater. 14 (2002) 3.
[55] Z. Luan, M. Hartmann, D. Zgao, W. Zhou and L. Kevan, Chem. Mater. 11 (1999) 1621.
[56] Y. Yue, A. Cedeon, J.-L. Bonardet, N. Melosh, J.-B. D'Esinose and J. Fraissard, Chem. Commun. (1999) 1697.
[57] Y. Han, S. Wu, Y. Sun, D. Li, F.-S. Xiao, J. Liu and X. Zhang, Chem. Mater. 14 (2002) 1144.
[58] Y.Y. Sun, Y. Han, L. Yuan, S.Q. Ma, D. Jiang and F.-S. Xiao, J. Phys. Chem. B. 107 (2003) 1853.
[59] F. Chen, M. Zhang, Yu Han, F.-S. Xiao, Y. Yue, C. Ye and F. Deng, J. Phys. Chem. B. in press.
[60] K. Miyazawa and S. Inagaki, Chem. Commun. (2000) 2121.
[61] Y. Han, N. Li, L. Zhao, D.F. Li, X.Z. Xu, S. Wu, Y. Di and F.-S. Xiao, J. Phys. Chem. B 107 (2003) 7551.
[62] J. Fraissard and T. Ito, Zeolites 8 (1988) 350.
[63] J.L. Bonardet, J. Fraissard, A. Dedeon and M. A. Springuel-Huet, Catal. Rev-Sci. Eng. 41 (1999) 115.
[64] M.-A. Springuel-Huet, K. Sun and J. Fraissard, Microporous Mesoporous Mater. 33 (1999) 89.
[65] *Cerius2;* Molecular Simulation/Biosysm Corporation: San Diego, CA,1995.
[66] J. Liu, X. Zhang, Y. Han and F.-S. Xiao, Chem. Mater. 14 (2002) 2536.

[67] P. E. A. de Moor, T. P. M. Beelen and R. A. van Santen, J. Phys. Chem, B 103 (1999) 1639.
[68] M. Taramasso, G. Perego and B. Notari, US Patent 4410501, 1983..
[69] Z. Tuel, Zeolites 15 (1995) 236.
[70] D.P. Serrano, H.X. Li, and M.E. Davis, Chem. Commun. (1992) 745.
[71] T. Blasco, M.A. Camblor, A. Corma and J. Perez-Pariente, J. Am. Chem. Soc. 115 (1993) 11806.
[72] D.R.C. Huybrechts, L. De Bruycker and P.A. Jabobs, Nature 345 (1990) 240.
[73] B. Notari, Structure–Activity and Selectivity Relationship in: *Heterogeneous Catalysis*, eds. R.K. Grasselli and A.W Sleight Vol. 243, (Elsevier, Amsterdam, 1991).
[74] P.T. Tanev, M. Chibwe and T.J. Pinnavaia, Nature 368 (1994) 321; W. Zhang, J. Wang, P.T. Tanev and T.J. Pinnavia, Chem. Commun. (1996) 979.
[75] S. Inagaki, Y. Fukushima and K. Kuroda, Chem. Commun. (1993) 680.
[76] K.A. Koyano and T. Tatsumi, Chem. Commun. (1996) 145.
[77] A. Corma, M.T. Navarro and J. Perez Pariente, Chem. Commun. (1994) 147.
[78] T. Blasco, A. Corma, M.T. Navarro and J. Perez Pariente, J. Catal. 156 (1995) 65.
[79] L.N. Bharat, O. Johnson and K. Sridhar, Chem. Mater. 13 (2001) 552.
[80] T. Maschmeyer, F. Rey, G. Sankar and J.M. Thomas, Nature 378 (1995) 159.
[81] M.J. Maclachlan, N. Coombs and G.A. Ozin, Nature 397 (1999) 681.
[82] X. Xu, M.S. Thesis, Jilin University, China, 1999.
[83] F.-S. Xiao, Y. Han, Y. Yu, X.J. Meng, M. Yang and S. Wu, J. Am. Chem. Soc. 124 (2002) 888.
[84] X.-J. Meng, D.-F. Li, X.Y. Yang, Y. Yu, S. Wu, Y. Han, Q. Yang, D.Z. Jiang and F.-S. Xiao, J. Phys. Chem. 107 (2003) 8972.
[85] C. Li, G. Xiong, Q. Xin, J. Liu, P. Ying, Z. Feng, J. Li, W. Yang, Y. Wang, G. Wang, X. Liu, M. Lin, X. Wang and E. Min, Angew. Chem. Int. Ed. 38 (1999) 2220.
[86] K. Lin, D. Jiang and F.-S. Xiao, unpublished results.
[87] M. Y. He and E. Min, Proceedings of 10th National Meeting on Catalysis, Hunan, China, October 2000.
[88] J.S. Beak, J.C. Vartuli, G.J. Kennedy, C.T. Kresge, W.J. Roth and S.E. Schramm, Chem. Mater. 6 (1994) 1816.
[89] R. Mokaya, J. Phys. Chem. B 103 (1999) 10204.
[90] Y. Muto, K. Esumi, K. Meguro, R. Zana, J. Colloid Interface Sci. 120 (1987) 162.
[91] H. Matsubara, S. Muroi, M. Kameda, N. Ikeda, A. Ohta and M. Aratono, Langmuir 17 (2001) 7752.
[92] J. Penfold, E. Staples, L. Thompson, I. Tucker, J. Hines, R.K. Thomas, J.R. Lu and N. Warren, J. Phys. Chem. B 103 (1999) 5204.
[93] Y. Han, D. Li, L. Zhao, J. Song, X. Yang, N. Li, Y. Di, C. Li, S. Wu, X. Xu, X. Meng, K. Lin and F.-S. Xiao, Angew. Chem. Int. Ed. 42 (2003) 3633.
[94] R. Ryoo, C.H. Ko, M. Kruk, M. Antochshuk and M. Jaroniec, J. Phys. Chem. B 104 (2000) 11465